

Learning Green's Functions of Linear Reaction-Diffusion Equations with Application to Fast Numerical Solver

Yuankai Teng¹, Xiaoping Zhang², Zhu Wang¹ and Lili Ju¹

¹Department of Mathematics, University of South Carolina, USA

²School of Mathematics and Statistics, Wuhan University, China

yteng@email.sc.edu, xpzhang.math@whu.edu.cn, wangzhu@math.sc.edu, ju@math.sc.edu

Abstract

Partial differential equations are often used to model various physical phenomena, such as heat diffusion, wave propagation, fluid dynamics, elasticity, electrodynamics and image processing, and many analytic approaches or traditional numerical methods have been developed and widely used for their solutions. Inspired by rapidly growing impact of deep learning on scientific and engineering research, in this paper we propose a novel neural network, GF-Net, for learning the Green's functions of linear reaction-diffusion equations in an unsupervised fashion. The proposed method overcomes the challenges for finding the Green's functions of the equations on arbitrary domains by utilizing physics-informed approach and the symmetry of the Green's function. As a consequence, it particularly leads to an efficient way for solving the target equations under different boundary conditions and sources. We also demonstrate the effectiveness of the proposed approach by experiments in square, annular and L-shape domains.

1 Introduction

The success of deep learning algorithms in classifying images has promoted the data science study and the relevant researches of extending them to other fields in science and engineering. Those work has shown increasing impacts on many subjects including dynamical systems and partial differential equations (PDEs), thanks to the integration of available big data, effective learning algorithms and unprecedented computing powers. Consequently, the synthesis of deep learning techniques and numerical solution of PDEs has become an emerging research topic. Numerical techniques used in solving PDEs have been used to understand and further improve the network structure and settings. For example, the connection between multigrid methods and convolutional neural networks (CNNs) was discussed in [He and Xu, 2019] and MGNet was proposed to incorporate them. A discrete hyper-diffusion operator was used in [Osher *et al.*, 2018] to smooth the gradient of stochastic gradient descent methods in machine learning models including deep learning networks (DNNs). On the other hand,

using deep learning techniques to solve the PDEs has been studied in several recent work, and some of typical methods include the physics-informed neural networks (PINNs) [Raissi *et al.*, 2019], the deep Ritz method (DRM) [E and Yu, 2018], the deep Galerkin method (DGM) [Sirignano and Spiliopoulos, 2018] and PDE-Net [Long *et al.*, 2018]. The first three are meshfree and trained with the unsupervised fashion and the last one uses rectangular meshes and ground-truth for supervised training. Meanwhile, deep learning based methods has also been applied to construct computational surrogates for PDE models in [Khoo *et al.*, 2017; Nagoor Kani and Elsheikh, 2017; Nabian and Meidani, 2018; Lee and Carlberg, 2020; San *et al.*, 2019; Mücke *et al.*, 2019].

The ultimate goal of this paper is to design a neural network for fast solutions to a given linear reaction-diffusion equation defined on an arbitrary domain, that could yield an accurate response to different sources and initial/boundary conditions. To achieve this, we first propose a GF-Net that determines the Green's functions associated with the target differential equation. Once the network is well trained, it would accurately approximate the Green's functions, then the target PDEs subject to different boundary conditions and sources could be solved in an efficient manner. How to obtain Green's functions for general problems is a classic problem. The analytic formula of Green's functions are only known for few operators on either open spaces or domains with simple geometry. Finding their numerical approximations by traditional numerical methods turns out to be too expensive to be feasible in terms of computation and memory. The high dimensional parameter space also makes it almost impossible to use model reduction to find an efficient surrogate for the Green's functions. Therefore, the neural network architecture, GF-Net, proposed in this work provides a new way to tackle this classic problem through deep learning.

In particular, our GF-Net is physics-informed: a forward neural network is trained by minimizing the loss function measuring the pointwise residuals, discrepancy in initial/boundary values, and an additional term for penalizing the symmetry of the Green's function due to its underlying property of symmetry. Meanwhile, to accelerate the training process, we design a sampling strategy based on the position of the point source, and we further put forth a domain decomposition approach to train a multiple of GF-Nets in parallel on many blocks. Finally, the application of the GF-Nets

as fast solver of linear reaction-diffusion equations with different boundary conditions and sources is investigated. It is observed that the approach could yield decent numerical solutions by using the Green's function represented by GF-Nets.

2 Related work

Using neural networks to solve differential equations has been investigated in several early work, e.g., [Dissanayake and Phan-Thien, 1994; Lagaris *et al.*, 1998]. Recent advances in deep learning algorithms stimulate new exploration in this direction. The physics-informed neural networks (PINNs) developed in [Raissi *et al.*, 2019] represents the mapping from spatial/temporal variables to the state of the system by DNNs, which is then trained by minimizing mean squares of the residuals of PDEs at randomly selected interior points and the errors at initial/boundary points. This approach later has been extended to solve inverse problems [Raissi *et al.*, 2018], fractional differential equations [Pang *et al.*, 2019], stochastic differential equations, and tasks about uncertainty quantification in [Nabian and Meidani, 2018; Yang *et al.*, 2018a; Zhang *et al.*, 2019a; Zhang *et al.*, 2019b; Yang *et al.*, 2018b]. Improved sampling strategies are considered in [Lu *et al.*, 2019; Anitescu *et al.*, 2019]. On the other hand, the deep Ritz method (DRM) developed in [E and Yu, 2018] considers the variational form of PDEs. In order to optimize the network, it combines the mini-batch stochastic gradient descent algorithms with numerical integrations. Variational form is also considered in weak adversarial networks [Zang *et al.*, 2019]. The deep Galerkin method (DGM) proposed in [Sirignano and Spiliopoulos, 2018] merges Galerkin methods and machine learning, that is specially designed for solving a class of high-dimensional free boundary PDEs. The above three learning methods use no meshes as opposed to traditional numerical methods and are trained in an unsupervised fashion. The PDE-Net in [Long *et al.*, 2018] proposes a stack of networks (δt -blocks) to advance the PDE solutions over a multiple of time steps. It recognizes the equivalence between convolutional filters and differentiation operators in rectangular meshes under the supervised training with ground-truth. The approach is further combined with a symbolic multilayer neural network for recovering PDE models in [Long *et al.*, 2019].

3 Reaction-diffusion equations and Green's functions

In this work, we consider the reaction-diffusion operator defined on the domain $\Omega \subset \mathbb{R}^d$ represented by

$$\mathcal{L}(u)(\mathbf{x}) := -\nabla \cdot (a(\mathbf{x}) \nabla u(\mathbf{x})) + r(\mathbf{x})u(\mathbf{x}), \quad (1)$$

where $a(\mathbf{x}) > 0$ is the diffusion coefficient and $r(\mathbf{x}) \geq 0$ the reaction coefficient. The corresponding reaction-diffusion problem reads:

$$\begin{cases} \mathcal{L}(u)(\mathbf{x}) = f(\mathbf{x}), & \mathbf{x} \in \Omega, \\ u(\mathbf{x}) = g(\mathbf{x}), & \mathbf{x} \in \partial\Omega, \end{cases} \quad (2)$$

where $f(\mathbf{x})$ is the given source term and $g(\mathbf{x})$ is the Dirichlet boundary condition. The Green's function $G(\mathbf{x}, \xi)$ rep-

resents the impulse response of the PDE subject to homogeneous Dirichlet boundary condition, that is, for any $\xi \in \Omega$,

$$\begin{cases} \mathcal{L}(G)(\mathbf{x}, \xi) = \delta(\mathbf{x} - \xi), & \mathbf{x} \in \Omega, \\ G(\mathbf{x}, \xi) = 0, & \mathbf{x} \in \partial\Omega. \end{cases} \quad (3)$$

Here, $\delta(\mathbf{x})$ is the Dirac delta function satisfying $\delta(\mathbf{x}) = 0$ if $\mathbf{x} \neq 0$ and $\int_{\mathbb{R}^d} \delta(\mathbf{x}) d\mathbf{x} = 1$. Note that the Green's function G is symmetric, i.e., $G(\mathbf{x}, \xi) = G(\xi, \mathbf{x})$.

If $G(\mathbf{x}, \xi)$ is known, equation (2) with different sources or boundary conditions can be immediately solved in the following format: for $\forall \mathbf{x} \in \Omega$,

$$\begin{aligned} u(\mathbf{x}) = & \int_{\Omega} f(\xi)G(\mathbf{x}, \xi) d\xi \\ & - \int_{\partial\Omega} g(\xi)a(\xi)(\nabla_{\xi} G(\mathbf{x}, \xi) \cdot \vec{n}_{\xi}) dS(\xi), \end{aligned} \quad (4)$$

where \vec{n}_{ξ} denotes the unit outer normal vector on $\partial\Omega$.

Note that the Green's functions on general domains don't have analytic formulas. We next introduce a deep learning approach to approximate the Green's function.

4 GF-Net: Learning Green's functions

We will construct a *deep feedforward network*, GF-Net, to learn the Green's function, and then use it for developing a fast solver to equation (2) based on the formula (4). We make use of a *fully connected neural network*, instead of convolutional neural network, because the latter is usually popular in image applications in order to extract local characteristic features from the data, but not for PDEs on arbitrary domains.

4.1 Network architecture

In order to represent the Green's function obeying (3), we adopt the framework of PINN [Raissi *et al.*, 2019], but some modifications have to be accommodated. The architecture of GF-Net for a two dimensional problem is shown in Figure 1.

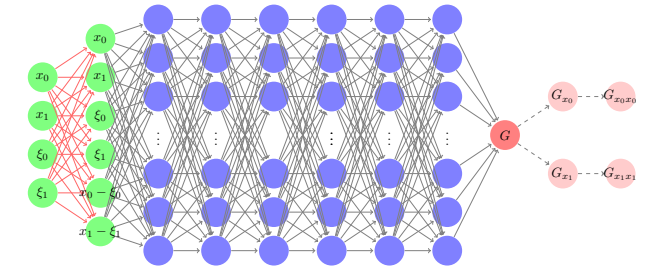


Figure 1: An illustration of the GF-Net architecture with 1 auxiliary layer (green) and 6 hidden layers (blue) for a 2-dimensional problem. The derivatives, such as G_{x_0} , $G_{x_0x_0}$, \dots , can be obtained by applying derivatives on G with respect to the inputs \mathbf{x} using automatic differentiation in the setting of Pytorch or Tensorflow.

The vector $\mathbf{v}^0 = [\mathbf{x} \ \xi]^T$ is fed as input to the network, followed by an auxiliary layer without bias and activation

$$\ell_0(\mathbf{x}, \xi) = \mathbf{W}_0 \begin{bmatrix} \mathbf{x} \\ \xi \end{bmatrix}, \quad \mathbf{W}_0 = \begin{bmatrix} \mathbf{I} & \mathbf{0} \\ \mathbf{0} & \mathbf{I} \\ \mathbf{I} & -\mathbf{I} \end{bmatrix}.$$

This is a preprocessing layer inspired by the formulation of the Greens' function containing the variables \mathbf{x} , ξ and $\mathbf{x} - \xi$. The layer is connected to $D - 1$ hidden layers and an output layer, which form a fully-connected neural network of depth D . Letting n_k be the number of neurons in the k -th layer, each hidden layer receives an input \mathbf{v}^{k-1} from the previous layer output and transforms it to

$$\ell_k(\mathbf{v}^{k-1}) = \mathbf{W}^k \mathbf{v}^{k-1} + \mathbf{b}^k. \quad (5)$$

The nonlinear activation function $\sigma(\cdot)$ is applied to each component of the transformed vector before sending it to the next layer, except the last hidden layer. The network thus is a composite of a sequence of nonlinear functions:

$$G(\mathbf{x}, \xi; \Theta) = (\ell_D \circ \sigma \circ \ell_{D-1} \circ \dots \circ \sigma \circ \ell_1 \circ \ell_0)(\mathbf{x}, \xi), \quad (6)$$

where the operator “ \circ ” denotes the composition and $\Theta = \{\mathbf{W}^k, \mathbf{b}^k\}_{k=1}^D$ represents the trainable parameters in the network. It should be noted that the weight \mathbf{W}^0 is frozen that need not to be updated during the training process.

4.2 Approximation of the Dirac delta function

In the network setting, we seek for a classic (smooth) solution satisfying the strong form of the PDE (3). However, $G(\mathbf{x}, \xi)$ is not everywhere differentiable as it is a response to the impulse source defined by the Dirac delta function. Indeed, it can only be well defined in the sense of distribution. Thus, in practice, we approximate the Dirac delta by a multidimensional Gaussian density function $\rho(\mathbf{x}, \xi) = \frac{1}{(\sqrt{2\pi}s)^d} e^{-\frac{|\mathbf{x}-\xi|^2}{2s^2}}$, where the parameter $s > 0$ denotes the standard deviation of the distribution. As $s \rightarrow 0$, this function approaches to the Dirac delta function.

4.3 Sampling point set generation

Both \mathbf{x} and ξ should be fed into the GF-Net. How to sample them can be flexible, for instance, the Latin hypercube sampling (LHS) could be used [Raissi *et al.*, 2019]. To make the sampling more effective, we put forth the following strategy: Since the spatial domain Ω may have complex geometrical shape, we adopt a mesh generator to first partition Ω into a triangular mesh $\mathcal{T}_\xi = (\mathcal{V}_\xi, \mathcal{E}_\xi)$ where \mathcal{V}_ξ denotes the vertex set and \mathcal{E}_ξ denotes the edge set, and then collect ξ -samples from the interior vertices to form $\mathcal{S}_\xi = \{\xi \in \mathcal{V}_\xi : \xi \notin \partial\Omega\}$. For each fixed ξ , we select \mathbf{x} -samples that concentrate around it because the Gaussian density function centers at ξ . Hence, we generate another three meshes $\{\mathcal{T}_x^i = (\mathcal{V}_x^i, \mathcal{E}_x^i)\}_{i=1}^3$ of resolutions from high to low, and collect \mathbf{x} -samples to form the set $\mathcal{S}_{\mathbf{x}, \xi} = \mathcal{S}_{\mathbf{x}, \xi}^1 \cup \mathcal{S}_{\mathbf{x}, \xi}^2 \cup \mathcal{S}_{\mathbf{x}, \xi}^3$, in which $\mathcal{S}_{\mathbf{x}, \xi}^1 = \{\mathbf{x} \in \mathcal{V}_x^1 : \|\mathbf{x} - \xi\|_\infty \leq c_1 s\}$, $\mathcal{S}_{\mathbf{x}, \xi}^2 = \{\mathbf{x} \in \mathcal{V}_x^2 : c_1 s < \|\mathbf{x} - \xi\|_\infty < c_2 s\}$, $\mathcal{S}_{\mathbf{x}, \xi}^3 = \{\mathbf{x} \in \mathcal{V}_x^3 : \|\mathbf{x} - \xi\|_\infty \geq c_2 s\}$ and c_1, c_2 are two hyperparameters. Finally, the overall dataset is selected as

$$\mathcal{S} = \{(\mathbf{x}, \xi) : \xi \in \mathcal{S}_\xi, \mathbf{x} \in \mathcal{S}_{\mathbf{x}, \xi}\}.$$

To highlight this sampling strategy, we plot in Figure 2 the \mathbf{x} -samples associated to a given ξ in three domains (square, annular and L-shape) we considered in numerical tests. In all experiments, we adopt the mesh generator [Ju, 2005] but any other good sampling/meshing method can be instead used here too.

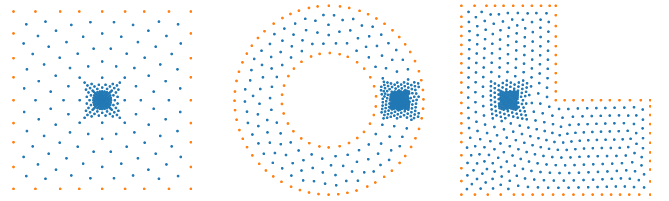


Figure 2: Locally refined \mathbf{x} -samples for a given ξ . Left: $\xi = (0, 0) \in \Omega_1$; middle: $\xi = (\frac{3}{4}, 0) \in \Omega_2$; right: $\xi = (-\frac{1}{2}, 0) \in \Omega_3$.

4.4 Partitioning strategy

Ideally, we wish to use a single GF-Net to model the Green's function associated to any ξ , but such a network may easily become unmanageable due to a large amount data in \mathcal{S} , or be difficult to train as different ξ may yield totally different behavior of the Green's function. Since the Green's functions corresponding to different ξ can be solved individually, one could possibly train a GF-Net for each sample ξ , which however would cause storage issues. Therefore, we propose a domain decomposition strategy to train a set of GF-Nets on ξ -blocks. Taking a two-dimensional domain Ω for example, we first find the circumscribed rectangle of Ω , then divide it into $m \times n$ blocks uniformly. Suppose there are $K \leq m \times n$ blocks containing samples of ξ , we denote the ξ -sample set in the k -th block by \mathcal{S}_ξ^k , for $k = 1, \dots, K$. Consequently, we define the sample set associated to the k -th ξ -block by $\mathcal{S}^k = \{(\mathbf{x}, \xi) : \xi \in \mathcal{S}_\xi^k, \mathbf{x} \in \mathcal{S}_{\mathbf{x}, \xi}\}$.

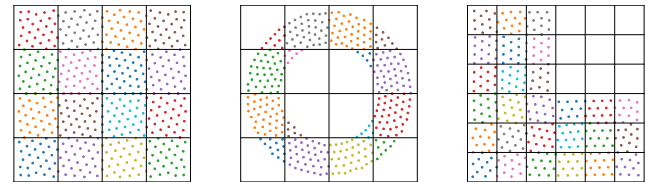


Figure 3: Uniform sampling on three domains and partitioning ξ in blocks. Left: 4×4 ; middle: 4×4 ; and right: 6×6 .

Based on the new partitioned samples, a set of K GF-Nets will be independently trained. The approach has at least two advantages: firstly, the training tasks are divided into many small subtasks, that are naturally parallelizable and can be distributed to many GPUs for efficient implementations; secondly, because the models are trained locally, their generalization ability tends to be stronger than the global model.

4.5 Loss function

Define $\mathcal{S}^k = \mathcal{S}_c^k \cup \mathcal{S}_b^k$, where $\mathcal{S}_c^k = \{(\mathbf{x}, \xi) \in \mathcal{S}^k : \mathbf{x} \notin \partial\Omega\}$ and $\mathcal{S}_b^k = \{(\mathbf{x}, \xi) \in \mathcal{S}^k : \mathbf{x} \in \partial\Omega\}$, for $k = 1, \dots, K$. The k -th GF-Net is trained by minimizing the following loss:

$$L(\Theta_k) = L_{res}(\Theta_k) + \lambda_b L_{bdry}(\Theta_k) + \lambda_s L_{sym}(\Theta_k), \quad (7)$$

$$\text{where } L_{res}(\Theta_k) = \frac{1}{|\mathcal{S}_c^k|} \sum_{(\mathbf{x}, \xi) \in \mathcal{S}_c^k} [\mathcal{L}G(\mathbf{x}, \xi; \Theta_k) - \rho(\mathbf{x}, \xi)]^2,$$

$$L_{bdry}(\Theta_k) = \frac{1}{|\mathcal{S}_b^k|} \sum_{(\mathbf{x}, \xi) \in \mathcal{S}_b^k} [G(\mathbf{x}, \xi; \Theta_k)]^2,$$

$$L_{sym}(\Theta_k) = \frac{1}{|\mathcal{S}_c^k|} \sum_{(\mathbf{x}, \xi) \in \mathcal{S}_c^k} [G(\mathbf{x}, \xi; \Theta_k) - G(\xi, \mathbf{x}; \Theta_k)]^2.$$

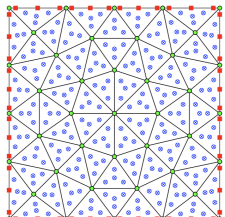
Here, $L_{res}(\Theta_k)$ represents the pointwise PDE residual, L_{bdry} measures the boundary errors, $L_{sym}(\Theta_k)$ is introduced to enforce the intrinsic symmetry property of the Green's function, and λ_b and λ_s are two hyperparameters for balancing the three terms. Note that the loss function (7) does not use any ground-truth data (i.e., the exact or certain approximate solution of equation (3)).

5 Fast PDE solver using GF-Nets

After training the set of GF-Nets, we then use them to compute numerical solutions of the reaction-diffusion problem (2) based on the formula (4). Note that the formula (4) involves integrations, in order to evaluate them accurately, we apply numerical quadratures on triangular meshes. To this end, we generate a triangulation for the domain Ω consisting of triangles $\mathcal{T}_q = \{T_l\}$. Denote the intersection of the triangle edges with the domain boundary by $\mathcal{E}_q^{bdry} = \{E_m\}$. Then for any $\mathbf{x} \in \Omega$, we have

$$\begin{aligned} u(\mathbf{x}) \approx & \sum_{T_l \in \mathcal{T}_q} I_{\xi, h}^{T_l} [f(\xi) G(\xi, \mathbf{x})] \\ & - \sum_{E_m \in \mathcal{E}_q^{bdry}} I_{\xi, h}^{E_m} [g(\xi) a(\xi) (\nabla_\xi G(\xi, \mathbf{x}) \cdot \vec{n}_\xi)], \end{aligned} \quad (8)$$

where $I_{\xi, h}^{T_l}[\cdot]$ denotes the numerical quadrature for evaluating $\int_{T_l} f(\xi) G(\mathbf{x}, \xi) d\xi$ and $I_{\xi, h}^{E_m}[\cdot]$ the quadrature for evaluating $\int_{E_m} g(\xi) a(\xi) (\nabla_\xi G(\mathbf{x}, \xi) \cdot \vec{n}_\xi) dS(\xi)$, respectively. For clarity, in Figure 4, we plot the quadrature points used in $I_{\xi, h}^{T_l}[\cdot]$ by a 4-point Gaussian quadrature rule for triangular elements and in $I_{\xi, h}^{E_m}[\cdot]$ by a 3-point Gaussian quadrature rule on boundary segments. Note that due to the symmetry of $G(\xi, \mathbf{x})$, (8) can also be rewritten as an integration with respect to \mathbf{x} instead of ξ . The algorithm for solving the PDE by GF-Nets is summarized in Algorithm 1.



- the interior vertices of mesh, i.e., \mathbf{x} in (8);
- quadrature points in triangular elements in \mathcal{T}_q ;
- quadrature points on boundary edges in \mathcal{E}_q^{bdry} .

Figure 4: An illustration of a quadrature mesh \mathcal{T}_q and the quadrature points in the element and on the boundary.

6 Experimental results

In this section, we will investigate the performance of the proposed GF-Nets for approximating the Green's functions and solving the target PDEs. Every GF-Net (on each block) in the experiments has 1 auxiliary layer and 6 hidden layers with 50 neurons per layer, $\sigma(\mathbf{x}) = \sin(\mathbf{x})$ is used as the activation function, $\lambda_b = 400$ and $\lambda_s = 1$ are taken in the loss function if not specially specified, and $s = 0.02$ is taken in the Gaussian density function for approximate the Delta function. Both the Adam and LBFGS optimizers are used in the

Algorithm 1: Solving PDEs by GF-Nets

Input: The PDE data Ω , $\mathcal{L}(\cdot)$, $f(\mathbf{x})$ and $g(\mathbf{x})$, a mesh \mathcal{T}_q for quadrature rule, any interior vertex $\hat{\mathbf{x}} \in \Omega$
Output: The PDE solution $u(\hat{\mathbf{x}})$

- 1 Generate sampling points \mathcal{S}_ξ and $\mathcal{S}_{\mathbf{x}, \xi}$;
- 2 Apply the domain partition to divide Ω into K blocks;
- 3 **while** $k = 1, \dots, K$ **do**
 - 4 Collect the dataset in the k -th ξ -block
 - $\mathcal{S}^k = \{(\mathbf{x}, \xi) : \xi \in \mathcal{S}_\xi^k, \mathbf{x} \in \mathcal{S}_{\mathbf{x}, \xi}\}$;
 - 5 Train the GF-Net $G(\mathbf{x}, \xi; \Theta_k)$ by feeding all $(\mathbf{x}, \xi) \in \mathcal{S}^k$;
- 6 Check index k of the ξ -block which $\hat{\mathbf{x}}$ locates in, $u(\hat{\mathbf{x}})$ is computed from (8) using the $G(\mathbf{x}, \xi; \Theta_k)$.

training process. The purpose of the former is to provide a good initial guess to the latter. The Adam is run for up to 10^4 steps with the training loss tolerance $\epsilon_1 = 0.5$ for possible early stopping, which is then followed by the LBFGS optimization for at most 2×10^4 steps with the loss tolerance $\epsilon_2 = 1 \times 10^{-4}$. The same setting is used in training all GF-Nets for ensuring them to possess the same level of accuracy.

To test the ability of the GF-Net for approximating the Green's functions, we consider both the Poisson's (pure diffusion) equations and a reaction-diffusion equation on the square domain $\Omega_1 = [-1, 1]^2$, the annular domain $\Omega_2 = O_1(\mathbf{0}) \setminus O_{1/2}(\mathbf{0})$ with $O_r(\mathbf{0})$ denoting a circle centered at the origin with radius r and the L-shape domain $\Omega_3 = [-1, 1]^2 \setminus [0, 1]^2$, as shown in Figure 3. The numerical solutions of the PDEs at all the interior vertices \mathcal{V}_q of the triangulation \mathcal{T}_q are used for quantifying the performance, which are measured by the relative error in the L_2 norm defined by

$$e_2 = \frac{\left(\sum_{\mathbf{x} \in \mathcal{V}_q} |u_e(\mathbf{x}) - u_p(\mathbf{x})|^2 A_{\mathbf{x}} \right)^{1/2}}{\left(\sum_{\mathbf{x} \in \mathcal{V}_q} |u_e(\mathbf{x})|^2 A_{\mathbf{x}} \right)^{1/2}},$$

where $A_{\mathbf{x}}$ is the area of the dual cell related to the vertex \mathbf{x} , u_e and u_p denote the exact solution and approximate solution, respectively. The Gaussian quadrature rules with 4 points on triangular elements and 3 points on boundary segments are used in all numerical integrations.

6.1 Ablation study for Poisson's equation on Ω_1

We will study the effect of (i) the partitioning strategy and (ii) symmetry constraints in this subsection. Therefore, we first use the Poisson's equation (that is pure diffusion, $a(\mathbf{x}) = 1$ and $r(\mathbf{x}) = 0$ in (1)) on the square domain Ω_1 as a test for ablation study. Two cases are considered: Case I is with homogeneous Dirichlet BC, in which the exact solution $u(x, y) = \sin(2\pi x) \sin(2\pi y)$ and $f(x, y) = 8\pi^2 u(x, y)$; Case II is of inhomogeneous Dirichlet BC, in which $u(x, y) = 2x^2 + y^2 + 1$, $f(x, y) = -6$, and $g(x, y)$ matches the exact solution on the boundary.

For ξ -samples, we choose the mesh \mathcal{T}_ξ with $\#\mathcal{V}_\xi = 545$. The related \mathbf{x} -samples are selected from three meshes

$\{\mathcal{T}_x^i\}_{i=1}^3$ with $\#\mathcal{V}_x^1 = 32753$, $\#\mathcal{V}_x^2 = 8265$, $\#\mathcal{V}_x^3 = 2105$, and $c_1 = 5$, $c_2 = 10$ to generate the sampling point set \mathcal{S} .

(i) Partitioning strategy

We test the impact of partitioning strategy in GF-Nets on the numerical solutions by considering 4×4 , 5×5 and 6×6 blocks. Here $\lambda_s = 0$ is chosen in the loss function (i.e., the symmetry constraint is not imposed). For the 4×4 case, the predicted Green's function at $\xi = (-0.8, 0.8)$ is shown in Figure 5 (left). The time taken on each block during the training process are reported in Figure 6. It is observed that: 1) the training on blocks away from corners and boundaries of the domain are generally faster. In fact, the training processes for all interior blocks terminate early within thousands of LBFGS steps; 2) the training time per block decreases as the number of blocks increases, which implies this strategy is suitable for parallel training when many GPU cards are available.

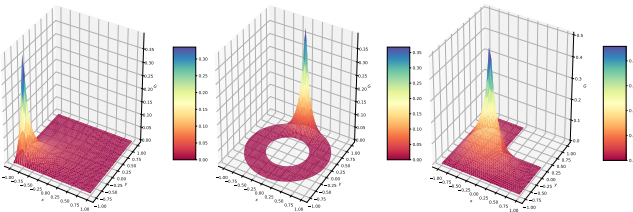


Figure 5: Predicted Green's functions $G(\mathbf{x}, \xi)$ of the Poisson's equation on Ω_1 at $\xi = (-0.8, -0.8)$ (left), on Ω_2 at $\xi = (0, 0.8)$ (middle), and on Ω_3 at $\xi = (-0.2, -0.2)$ (right).

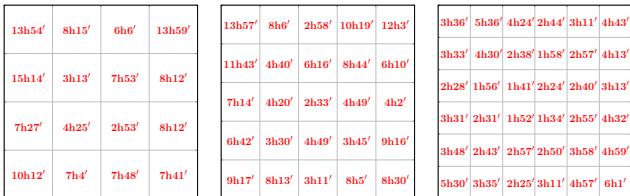


Figure 6: Training time on each block for 4×4 (left), 5×5 (middle) and 6×6 partitions (right).

The trained GF-Net is then applied for solving the Poisson's equations. Three quadrature meshes are considered and the resulted solution errors are listed in Table 1. It is seen that when different partitions are used, the numerical accuracy remains at the same level (around 1.0×10^{-2}) with some slight improvements for larger partitions in both cases.

# \mathcal{V}_q	Case I			Case II		
	4×4	5×5	6×6	4×4	5×5	6×6
145	9.74e-3	9.73e-03	9.34e-3	1.07e-2	9.91e-03	8.93e-3
289	9.37e-3	9.25e-03	8.73e-3	1.11e-2	9.06e-03	8.67e-3
545	1.26e-2	1.21e-02	1.19e-2	9.40e-3	8.58e-03	8.81e-3

Table 1: Numerical errors of the predicted solutions to the Poisson's equation on Ω_1 when different partitions are used and the symmetry constraint is not included in the loss.

(ii) Symmetry constraints

Keeping the same model setting, we then turn the hyperparameter $\lambda_s = 1$ (i.e., include the symmetry loss), train GF-Nets again and rerun the simulations. To show the influence

of the symmetry constraint on the training process, we plot the evolution of the three loss terms in Figure 7, compared with the $\lambda_s = 0$ case. From it, we observe that: 1) the symmetry constraint accelerates the decrease of both L_{res} and L_{bdry} ; 2) when $\lambda_s = 0$, the trained Green's functions have weaker symmetry, thus L_{sym} will not decay.

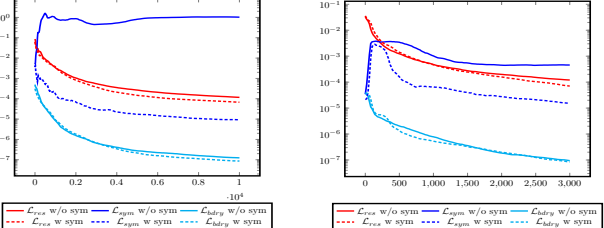


Figure 7: Evolutions of the loss terms during the training process in a corner block (left) and a center block (right) when $\lambda_s = 0$ (w/o sym) or 1 (w sym).

# \mathcal{V}_q	Case I			Case II		
	4×4	5×5	6×6	4×4	5×5	6×6
145	9.97e-3	9.63e-3	8.67e-3	8.34e-3	8.83e-3	7.18e-3
289	9.42e-3	8.91e-3	8.54e-3	7.74e-3	6.44e-3	6.76e-3
545	1.26e-2	1.19e-2	1.18e-2	7.10e-3	6.53e-3	6.92e-3

Table 2: Numerical errors of the predicted solutions to the Poisson's equation on Ω_1 when different partitions are used and the symmetry constraint is included in the loss.

The corresponding numerical errors for solving the PDEs are listed in Table 2 and the predicted results on 6×6 blocks are presented in Figure 8. Compared to the results in Table 1, it is observed that the GF-Nets with the symmetry constraint achieve close accuracy in the homogeneous BC case but clearly better accuracy in the inhomogeneous BC case.

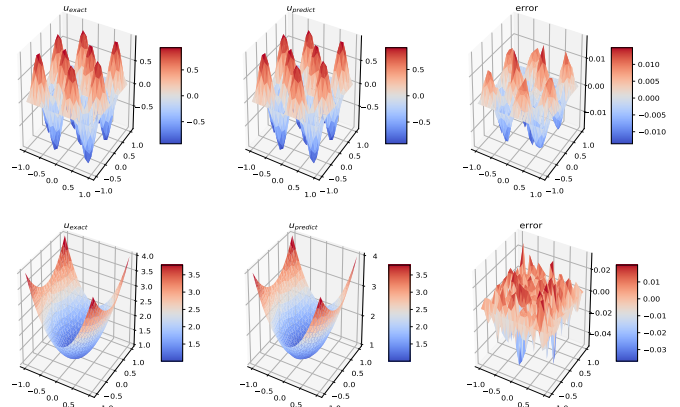


Figure 8: Numerical results in Case I (row 1) and Case II (row 2), showing the exact solutions (left), predicted solutions (middle) and numerical errors (right).

6.2 Poisson's equation on Ω_2 and Ω_3

To further test the performance of GF-Nets on non-convex domains, we consider the Poisson's equation on the annular domain Ω_2 and L-shape domain Ω_3 . We choose the same exact solutions as those (Cases I and II) in the last subsection. Some model parameters are listed in Table 3. The trained

Green's functions $G(\mathbf{x}, \xi)$ on Ω_2 at $\xi = (0, 0.8)$ and on Ω_3 at $\xi = (-0.2, -0.2)$ are shown in Figure 5 (middle and right), and numerical results evaluated by three quadrature meshes are displayed in Table 4. It is seen that: 1) GF-Nets are able to well approximate Green's functions on these two domains; 2) similar to the one in square domain, evaluating (8) on a finer quadrature mesh doesn't improve the accuracy significantly, which indicates the numerical error is dominated by Green's function approximation error. As an example, the numerical solutions to Case II are plotted in Figure 9.

Domain	$\#\mathcal{V}_\xi$	$\#\mathcal{V}_\alpha^1$	$\#\mathcal{V}_\alpha^2$	$\#\mathcal{V}_\alpha^3$	m	n	c_1	c_2
Ω_1	545	32753	8265	2105	4	4	5	10
Ω_2	493	27352	6981	1819	4	4	5	10
Ω_3	411	49663	6102	1565	6	6	5	10

Table 3: Parameter settings for all three domains.

Ω_2			Ω_3		
$\#\mathcal{V}_q$	Case I	Case II	$\#\mathcal{V}_q$	Case I	Case II
143	1.27e-2	2.72e-3	113	1.09e-2	1.47e-2
224	1.42e-2	5.53e-3	225	8.77e-3	1.52e-2
493	1.36e-2	2.16e-3	411	1.18e-2	1.22e-2

Table 4: Numerical errors of the predicted solutions to the Poisson's equation on Ω_2 and Ω_3 .

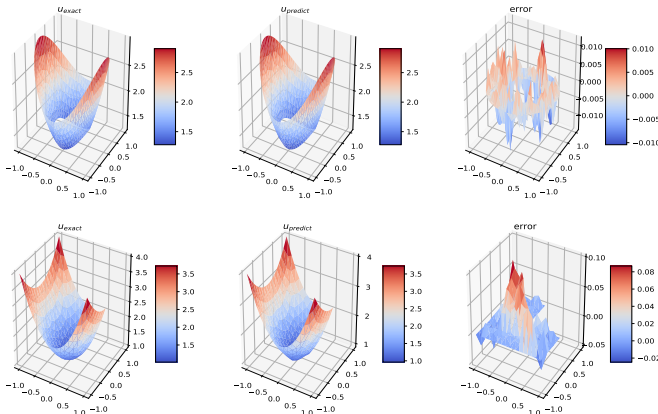


Figure 9: Poisson's equation on Ω_2 (the first row) and Ω_3 (the second row) for Case II: the exact solution (left), predicted solutions (middle), and numerical errors (right).

6.3 Reaction-diffusion equation

We next test the proposed method on the following reaction-diffusion operator with variable coefficients:

$$\mathcal{L}(u) = -\nabla \cdot ((1 + 2y^2)\nabla u) + (1 + x^2)u \quad (9)$$

on the same three different domains as above. The exact solution is chosen as $u(x, y) = e^{-(x^2+2y^2+1)}$ and the boundary conditions and source term are determined accordingly. We use the same parameters listed in Table 3. The predicted Green's functions $G(\mathbf{x}, \xi)$ are shown in Figure 10 for the problem on Ω_1 at $\xi = (-0.8, -0.8)$, Ω_2 at $\xi = (0, 0.8)$, and Ω_3 at $\xi = (-0.2, -0.2)$. Numerical results are reported in Table 5 and shown in Figure 11. It is observed that our method again achieves similar numerical performance as to the Poisson's equation.

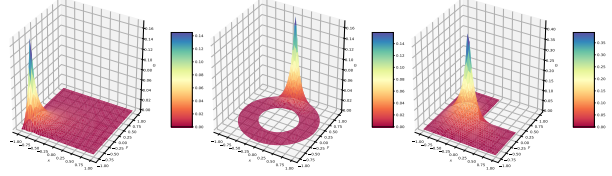


Figure 10: Predicted Green's functions $G(\mathbf{x}, \xi)$ of the reaction-diffusion equation on Ω_1 at $\xi = (-0.8, -0.8)$ (left), Ω_2 at $\xi = (0, 0.8)$ (middle) and Ω_3 at $\xi = (-0.2, -0.2)$ (right).

Ω_1		Ω_2		Ω_3	
$\#\mathcal{V}_q$	e_2	$\#\mathcal{V}_q$	e_2	$\#\mathcal{V}_q$	e_2
145	4.82e-3	143	7.89e-3	113	3.84e-2
289	4.52e-3	224	5.08e-3	225	4.56e-2
545	5.02e-3	493	2.24e-3	411	4.72e-2

Table 5: Numerical errors of the predicted solutions to the reaction-diffusion equation on Ω_1 , Ω_2 and Ω_3 , respectively.

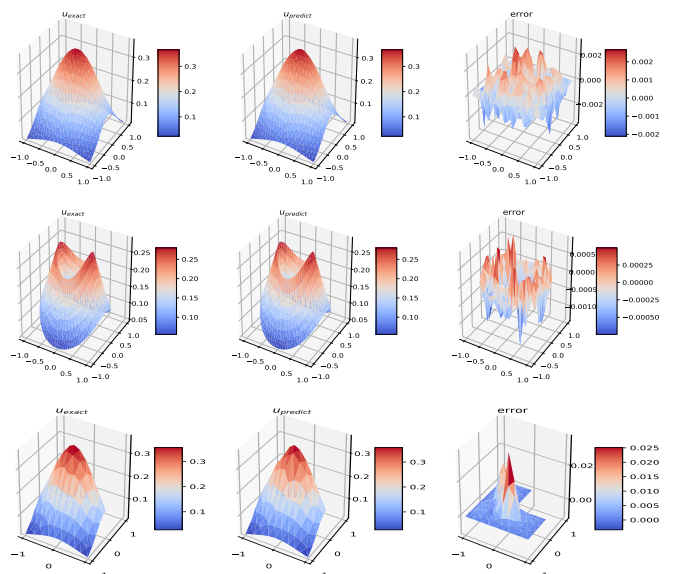


Figure 11: The reaction-diffusion equation on Ω_1 (row 1), Ω_2 (row 2) and Ω_3 (row 3): the exact solutions (left), predicted solutions (middle), and numerical errors (right).

7 Conclusion

In this paper, we have introduced “GF-Net” to learn the Green's functions of linear reaction-diffusion equations without supervision. Our method overcomes the challenges faced by classic and machine learning approaches in determining the Green's functions to differential operators on arbitrary domains. We take a series of procedures to embed underlying properties of the Green's functions in our network model. In particular, the symmetry feature is preserved by adding a penalization term in the loss function, and a domain decomposition approach is used for accelerating training and achieving better generalization. The trained GF-Nets are then used for fast numerical solution to the target PDEs under the help of numerical quadratures. Numerical tests have shown that the GF-Nets can handle well the reaction-diffusion equations on domains with arbitrary shapes. An interesting future work is to extend the proposed GF-Net to time-dependent PDEs.

References

[Anitescu *et al.*, 2019] Cosmin Anitescu, Elena Atroschenko, Naif Alajlan, and Timon Rabczuk. Artificial neural network methods for the solution of second order boundary value problems. *Computers, Materials & Continua*, 59(1):345–359, 2019.

[Dissanayake and Phan-Thien, 1994] MWMG Dissanayake and N Phan-Thien. Neural-network-based approximations for solving partial differential equations. *communications in Numerical Methods in Engineering*, 10(3):195–201, 1994.

[E and Yu, 2018] Weinan E and Bing Yu. The deep Ritz method: a deep learning-based numerical algorithm for solving variational problems. *Communication in Mathematics and Statistics*, 6, 2018.

[He and Xu, 2019] Junchai He and Jinchao Xu. MgNet: A unified framework of multigrid and convolutional neural network. *Science China Mathematics*, pages 1–24, 2019.

[Ju, 2005] Lili Ju. MESHGEN. http://people.math.sc.edu/ju/my_softwares/MESHGEN.tgz, 2005.

[Khoo *et al.*, 2017] Yuehaw Khoo, Jianfeng Lu, and Lexing Ying. Solving parametric pde problems with artificial neural networks. *arXiv preprint arXiv:1707.03351*, 2017.

[Lagaris *et al.*, 1998] Isaac E Lagaris, Aristidis Likas, and Dimitrios I Fotiadis. Artificial neural networks for solving ordinary and partial differential equations. *IEEE transactions on neural networks*, 9(5):987–1000, 1998.

[Lee and Carlberg, 2020] Kookjin Lee and Kevin Carlberg. Model reduction of dynamical systems on nonlinear manifolds using deep convolutional autoencoders. *Journal of Computational Physics*, 404, 2020.

[Long *et al.*, 2018] Zichao Long, Yiping Lu, Xianzhong Ma, and Bin Dong. PDE-Net: Learning PDEs from data. In *International Conference on Machine Learning*, pages 3214–3222, 2018.

[Long *et al.*, 2019] Zichao Long, Yiping Lu, and Bin Dong. PDE-Net 2.0: Learning PDEs from data with a numeric-symbolic hybrid deep network. *Journal of Computational Physics*, 399:108925, 2019.

[Lu *et al.*, 2019] Lu Lu, Xuhui Meng, Zhiping Mao, and George E Karniadakis. DeepXDE: A deep learning library for solving differential equations. *arXiv preprint arXiv:1907.04502*, 2019.

[Mücke *et al.*, 2019] Nikolaj Takata Mücke, Lasse Hjuler Christiansen, Allan Peter Karup-Engsig, and John Bagterp Jørgensen. Reduced order modeling for nonlinear pde-constrained optimization using neural networks. *arXiv preprint arXiv:1904.06965*, 2019.

[Nabian and Meidani, 2018] Mohammad Amin Nabian and Hadi Meidani. A deep neural network surrogate for high-dimensional random partial differential equations. *arXiv preprint arXiv:1806.02957*, 2018.

[Nagoor Kani and Elsheikh, 2017] J Nagoor Kani and Ahmed H Elsheikh. Dr-rnn: a deep residual recurrent neural network for model reduction. *arXiv preprint arXiv:1709.00939*, 2017.

[Osher *et al.*, 2018] Stanley Osher, Bao Wang, Penghang Yin, Xiyang Luo, Farzin Barekat, Minh Pham, and Alex Lin. Laplacian smoothing gradient descent. *arXiv preprint arXiv:1806.06317*, 2018.

[Pang *et al.*, 2019] Guofei Pang, Lu Lu, and George Em Karniadakis. fPINNs: Fractional physics-informed neural networks. *SIAM Journal on Scientific Computing*, 41(4):A2603–A2626, 2019.

[Raissi *et al.*, 2018] Maziar Raissi, Alireza Yazdani, and George Em Karniadakis. Hidden fluid mechanics: A Navier-Stokes informed deep learning framework for assimilating flow visualization data. *arXiv preprint arXiv:1808.04327*, 2018.

[Raissi *et al.*, 2019] Maziar Raissi, Paris Perdikaris, and George E Karniadakis. Physics-informed neural networks: A deep learning framework for solving forward and inverse problems involving nonlinear partial differential equations. *Journal of Computational Physics*, 378:686–707, 2019.

[San *et al.*, 2019] Omer San, Romit Maulik, and Mansoor Ahmed. An artificial neural network framework for reduced order modeling of transient flows. *Communications in Nonlinear Science and Numerical Simulation*, 77:271–287, 2019.

[Sirignano and Spiliopoulos, 2018] Justin Sirignano and Konstantinos Spiliopoulos. DGM: A deep learning algorithm for solving partial differential equations. *Journal of Computational Physics*, 375:1339–1354, 2018.

[Yang *et al.*, 2018a] Liu Yang, Dongkun Zhang, and George Em Karniadakis. Physics-informed generative adversarial networks for stochastic differential equations. *arXiv preprint arXiv:1811.02033*, 2018.

[Yang *et al.*, 2018b] Liu Yang, Dongkun Zhang, and George Em Karniadakis. Physics-informed generative adversarial networks for stochastic differential equations. *arXiv preprint arXiv:1811.02033*, 2018.

[Zang *et al.*, 2019] Yaohua Zang, Bao Gang, Xiaojing Ye, and Haomin Zhou. Weak adversarial networks for high-dimensional partial differential equations. *arXiv preprint arXiv:1907.08272*, 2019.

[Zhang *et al.*, 2019a] Dongkun Zhang, Ling Guo, and George Em Karniadakis. Learning in modal space: Solving time-dependent stochastic pdes using physics-informed neural networks. *arXiv preprint arXiv:1905.01205*, 2019.

[Zhang *et al.*, 2019b] Dongkun Zhang, Lu Lu, Ling Guo, and George Em Karniadakis. Quantifying total uncertainty in physics-informed neural networks for solving forward and inverse stochastic problems. *Journal of Computational Physics*, 397:108850, 2019.